Carrier relaxation dynamics in Sn_xN_y nanowires grown by chemical vapor deposition

Andreas Othonos[1,a)] and Matthew Zervos[2]
[1]*Department of Physics, Research Center of Ultrafast Science, University of Cyprus, P.O. Box 20537, Nicosia 1678, Cyprus*
[2]*Department of Mechanical Engineering, Nanostructured Materials and Devices Laboratory, P.O. Box 20537, Nicosia 1678, Cyprus*

(Received 21 July 2009; accepted 22 October 2009; published online 1 December 2009)

Carrier relaxation dynamics in tin nitride (Sn_xN_y) nanowires have been investigated using femtosecond transient absorption spectroscopy. The nanowires were grown directly on quartz using chemical vapor deposition and had diameters $\leq$200 nm and lengths up to 2 μm. Steady state optical transmission measurements suggest that the band gap is ~2.9 eV while time resolved measurements reveal that free carrier absorption dominates the carrier dynamics and overcomes state filling within 0.5 ps of the incoming excitation pulse even when probing above the band edge. This is a unique and markedly different behavior compared to what we have observed in other semiconductor nanowires and it is attributed to fast scattering of the photogenerated carriers out of the excitation energy region and possible rise in the lattice temperature due to energy relaxation. Carrier relaxation occurs through two channels with a fast time constants of $\approx$200 ps and a slow time constant ranging between 5 and 8 ns while intensity measurements reveal negligible contribution from nonlinear effects such as Auger recombination. © *2009 American Institute of Physics*. [doi:10.1063/1.3264721]

I. INTRODUCTION

Nitride (N) semiconductors and in particular group III-N compound semiconductors such as InN, GaN, and AlN have been studied extensively over the past decade due to their potential applications in devices such as field effect transistors, light emitting diodes, lasers, and other optoelectronic devices.[1–3] III-N semiconductors are especially attractive because their band gap can be tailored from 0.7 eV in InN (Ref. 4) up to 6.2 eV in AlN (Ref. 5). In contrast to group III-N compound semiconductors there are only few investigations on group IV-N compound semiconductors such as Ge_3N_4 (Ref. 6) and even less on Sn_3N_4.[7–19]

Tin nitride Sn_3N_4 is a relatively unknown semiconductor and the first investigation was carried out by Fisher and Iliovichi[7] back in 1908. So far Sn_3N_4 thin films have been grown by a variety of methods,[9–16] including atmospheric pressure chemical vapor deposition (APCVD) using halides,[9,10] metal-organic CVD,[11] sputtering,[12–14] and ammonothermal synthesis.[15,16] The band gap of the tin nitride films is not well determined, and has been reported to have values ranging from 1.5 (Ref. 8) to 4.9 eV (Ref. 11) depending on the growth method and conditions. In addition, thin films of Sn_3N_4 have been proposed as a medium for optical storage[17,18] since it was demonstrated that it dissociates into β-Sn upon exposure to a strong focused beam of light but also as a material for batteries.[19] Not surprisingly there are very few investigations on Sn_3N_4 nanostructured materials and so far only the synthesis of Sn_3N_4 nanoparticles on Au-coated Si(001) via CVD using $SnCl_4.5H_2O$ as a solid precursor has been achieved by Nand *et al.*[20] while more recently the authors reported on the synthesis of Sn_xN_y nanowires (NWs) on silicon.[21] To the best of our knowledge this was the first time that Sn_xN_y NWs were grown[21] despite the fact that semiconductor NWs constitute a fundamental building block for the development of nanoscale devices with various applications.

In order to complement our earlier investigations on the synthesis and properties of nitride NWs and related oxides[22–24] we have grown Sn_xN_y NWs with improved uniformity directly on quartz using APCVD in order to study carrier relaxation dynamics in this nanostructured material. Femtosecond pulse excitation was used to generate nonequilibrium carrier densities within the Sn_xN_y NWs and determine carrier relaxation through transient absorption measurements. We find that the free carrier absorption dominates the carrier dynamics and overcomes state filling within 0.5 ps of the excitation pulse even when probing above the band edge which is unique to Sn_xN_y NWs. Carrier relaxation occurs through two channels with a fast time constant of $\approx$200 ps and a slow time constant ranging between 5 and 8 ns while intensity measurements reveal negligible contribution of nonlinear effects such as Auger recombination for absorption fluences as high as 550 $\mu J/cm^2$. We discuss the possible origin for these effects.

II. EXPERIMENTAL PROCEDURE

The Sn_xN_y NWs were grown using an APCVD reactor which consists of four mass flow controllers and a horizontal quartz tube furnace capable of reaching a maximum temperature of 1100 °C. Initially fine Sn powder (Aldrich, $<$150 μm, 99.5%) was thoroughly mixed with anhydrous NH_4Cl (VWR Int 99.9%) at a ratio of 1:2 inside a porcelain

a)Electronic mail: othonos@ucy.ac.cy.

type boat and spread out over almost half of its length while a square piece of quartz $\approx 7 \times 7$ mm^2 in size, coated with 0.5 nm of Au was positioned approximately 5 mm downstream from the mixture, near the center. The Au layer was deposited via sputtering at a slow rate using an Ar plasma under a pressure $\approx 10^{-2}$ mbar. After loading the solid precursors and sample into the boat it was inserted into the reactor and positioned directly above the thermocouple used to measure the heater temperature (T_H) at the center of the quartz tube. Following this, a mixture of N_2 with 5% H_2 (99.999%) was introduced at a flow rate of 500 SCCM (SCCM denotes standard cubic centimeter per minute at STP) for 15 min in order to purge the tube and eliminate O_2 and H_2O. Then the temperature was ramped to the desired growth temperature (T_G) in a NH_3 flow of 250 SCCM at a rate of 10 °C/min after which the temperature was held constant for a further 60 min using 250 SCCM of NH_3 before allowing the reactor to cool down to room temperature again in a flow of 250 SCCM of NH_3. The sample was removed only when the temperature was lower than 100 °C.

The morphology of the NWs were examined with a TESCAN scanning electron microscope (SEM) while their crystal structure and phase purity were investigated using a SHIMADZU, XRD-6000, x-ray diffractometer with Cu-Ka source, by performing a scan of θ-2θ in the range between 10° and 80°. Steady state optical transmission was carried out using a Perkin Elmer Lambda 950 standard UV/V spectrophotometer at normal incidence while the dynamic behavior of carriers within the NWs was investigated through the temporal behavior of absorption obtained from simultaneous measurements of time resolved transmission and reflection.[22,25] The time resolved experiments were carried using a Ti:sapphire ultrafast amplifier system generating 45 fs pulses at 800 nm and running at a repetition rate of 5 kHz. Approximately 1 mJ of amplified energy was used to pump an optical parametric amplifier (OPA) providing ultrafast pulses in the UV range of the spectrum. The rest of the energy from the amplifier was used to generate 400 nm from a beta barium borate (BBO) crystal via second harmonic generation and white light super continuum. The UV femtosecond pulses from the OPA were used to excite the NWs. A small part of the fundamental pulses were used to generate VIS-IR super continuum light by focusing the beam on a 1-mm-thick sapphire plate. Similarly a super continuum light in the UV region of the spectrum was also generated using 400 nm pulses. The white light probe beam was used in a pump-probe noncollinear geometry, with the pump beam been generated from the OPA. To minimize the broadening of the laser pulse, optical elements such as focusing mirrors were utilized in the setup. The reflected and transmission probe beams were separately directed onto their respective detectors after passing through a bandpass filter and thus selecting the probe wavelength from the broadband white light. The differential reflected and transmission signals were measured using lock-in amplifiers with reference to the optical chopper frequency of the pump beam. The temporal variation in the photoinduced absorption was extracted using the transient reflection and transmission measurements, thus providing a means of monitoring the carrier dynamics within the probing region.

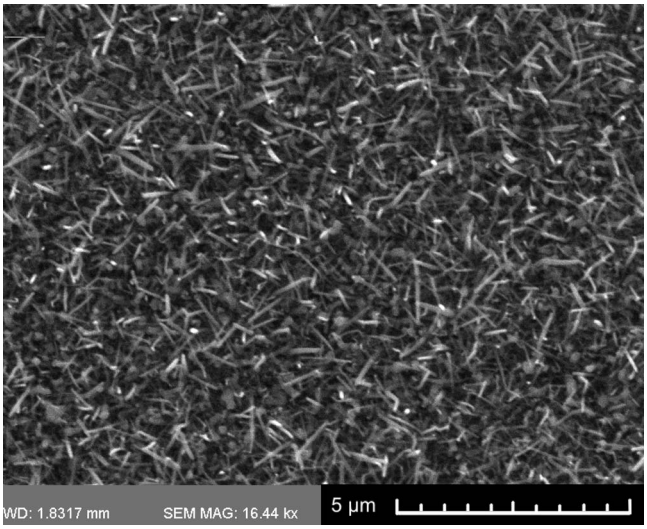

FIG. 1. Sn_xN_y NWs grown directly on quartz with 0.6 nm of Au at 425 °C using a ramp rate of 10 °C/min.

III. RESULTS AND DISCUSSION

A typical SEM image of the Sn_xN_y NWs grown on quartz is shown in Fig. 1. The Sn_xN_y NWs have diameters ≤ 200 nm and lengths up to 2 μm while their surface density was very uniform over the entire surface of the 7×7 mm^2 sample. The XRD spectrum of the Sn_xN_y NWs grown at 425 °C is shown in Fig. 2 and is characterized by the (2 2 0), (3 1 1), (5 1 1), and (4 4 0) peaks, which can be indexed to the hexagonal structure of Sn_xN_y.[15] As already discussed in detail elsewhere[21] the direct nitridation of Sn alone with NH_3 is not effective and one-dimensional growth is hindered by the formation of Sn droplets over a broad range of temperatures i.e., for T_G in the range of 300–800 °C. In contrast the growth of SnO_2 NWs via the oxidation of Sn in an inert gas flow of Ar at 800 °C occurs efficiently giving a high yield and uniformity of NWs without the formation of Sn droplets.[21] The formation of Sn droplets created by heating up Sn alone in a steady flow of NH_3 was overcome by the addition of NH_4Cl which undergoes sublimation at 338 °C and dissociates into NH_3 and HCl

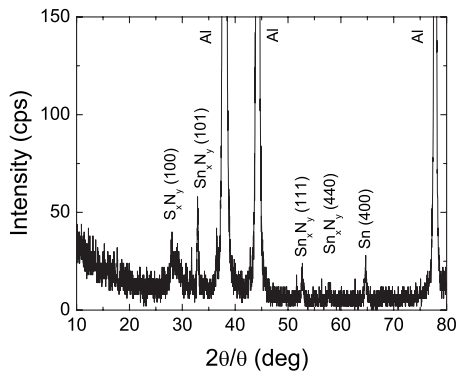

FIG. 2. XRD spectrum of the Sn_xN_y NWs grown at 425 °C.

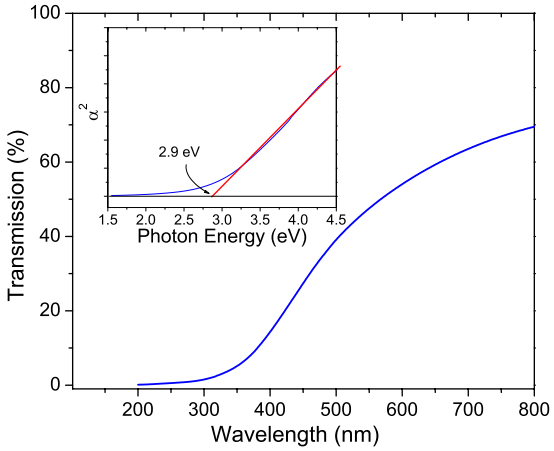

FIG. 3. (Color online) Optical transmission spectrum of Sn_xN_y NWs on quartz. The inset shows the square of the absorption vs energy providing an estimate for the band gap of the NWs. The extrapolated absorption edge is approximately 2.9 eV.

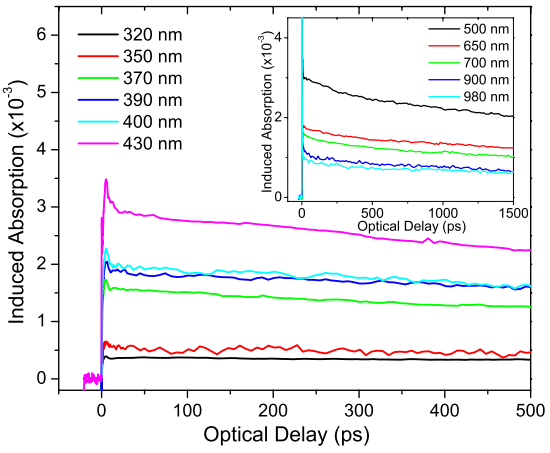

FIG. 4. (Color online) Time resolved differential absorption of Sn_xN_y NWs with excitation at 3.8 eV (320 nm) and probed using different probing wavelengths. The inset displays transient data for probing photon energies smaller than the band gap of this material.

thereby acting as a dispersant. As a consequence we obtained Sn_xN_y NWs at 450 °C under a steady flow of 250 SCCM of NH_3 using a ramp rate of 30 °C/min and a 1:1 ratio of Sn to NH_4Cl.[21] However the Sn_xN_y NWs were not distributed evenly across the surface of the sample and so the uniformity was poor. This nonuniform distribution of Sn_xN_y NWs was improved using a smaller ramp rate, i.e., 10 °C/min as opposed to 30 °C/min and larger amounts of NH_4Cl so that the Sn would be maintained spread out without forming droplets. This improvement in uniformity is a direct consequence of the steady, slow sublimation of NH_4Cl. A large temperature ramp rate, i.e., 30 °C/min leads to an abrupt and sudden onset in the sublimation of NH_4Cl and therefore a high degree of dispersion of the Sn in the boat which in turn results into a nonuniform distribution of NWs on the surface. In contrast small ramp rates, e.g., 10 °C/min lead to the gradual sublimation and dissociation of NH_4Cl which does not result into a strong dispersion of the Sn that starts melting at lower temperatures, i.e., 232 °C. The uniform distribution of the Sn_xN_y NWs was also confirmed from the optical properties which were found to be consistent across the surface of the sample.

Having obtained a uniform distribution of Sn_xN_y NWs on quartz we carried out steady state optical transmission measurements which suggest that the band gap is approximately 2.9 eV (Fig. 3). Furthermore, based on these measurements there is a clear indication of absorption below the band edge. This finite absorption corresponds to energy states within the band gap located between ≈2.0 eV from the top of the valence band.

In Fig. 4 we display typical time resolved differential absorption measurements for the Sn_xN_y NWs. The excitation femtosecond pulse was set at 3.8 eV (320 nm) with the fluence estimated to be 300 $\mu J/cm^2$. The probing photon energies cover the range above and below the band edge of this material. The x axis on this graph corresponds to the optical delay between the pump and the probe pulse whereas the y axis indicates the induced absorption. The behavior appears to be similar for all the probing wavelengths, where there seems to be an increase in the induced absorption reaching a maximum after a few picoseconds and then returning back to equilibrium over several nanoseconds. Here we should point out that when probing above the band edge there appears to be initially a decrease in the induced absorption which then recovers and becomes positive within ≈0.5 ps. Furthermore, to isolate above band edge dynamics transient absorption measurements were carried out with 3.1 eV (400 nm) photons corresponding to an excitation pulse just above the band edge. The measurements appear to have an identical behavior with the data seen in the inset of Fig. 4 where the excitation photons were 3.8 eV.

These observed changes in absorption are associated with the excitation of carriers by photons whose energy is larger than the band gap energy, resulting in the generation of nonequilibrium carrier densities and elevated carrier temperatures. As the system evolves toward equilibrium the photogenerated carriers distribute themselves along energy states that are normally unoccupied under equilibrium conditions. In our measurement this appears as a negative change in the induced absorption and is observed for probing photon energies larger than the band gap. At the same time a competing process known as "*free-carrier absorption*" is also likely to occur due to secondary excitation of the photogenerated carriers by the probing photons from their initial states to higher energy states. This phenomenon will result in a positive change in the induced absorption and depends on the number of carriers present at the initial states and the coupling coefficient between the two energy bands. When probing the NWs with above band edge photons, free-carrier absorption seems to overcome this effect within ≈0.5 ps, although initially it appears that state-filling occurs. This suggests that within this short time scale, photogenerated carriers move out of the excitation energy region, thus reducing the state filling effect and at the same time into energy states where free carrier absorption has a strong contribution. Free carrier contribution is further enhanced from an increase in the lattice temperature due to the relaxation of the photogenerated carriers. This overall dynamic behavior is unique and different from what has been observed in previous ultrafast spectroscopy in other semiconductor NWs (Ref. 22) where state

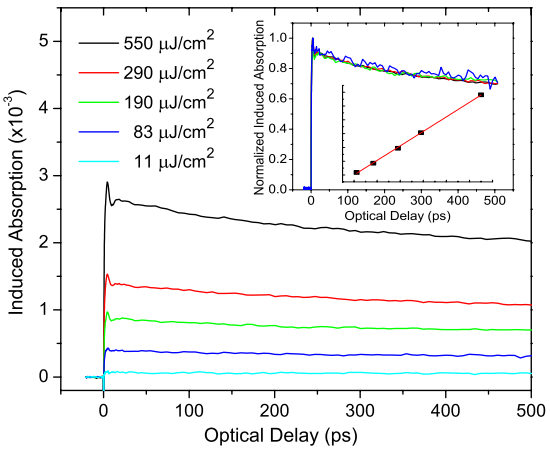

FIG. 5. (Color online) Transient absorption intensity measurements of the NWs at excitation of 3.8 eV (≡320 nm) and probing wavelength at 370 nm. The inset in the upper right corner corresponds to the same data normalized to clearly show the identical temporal evolution at all fluences. Also shown in the inset is the linear behavior of the induced absorption with increasing fluences.

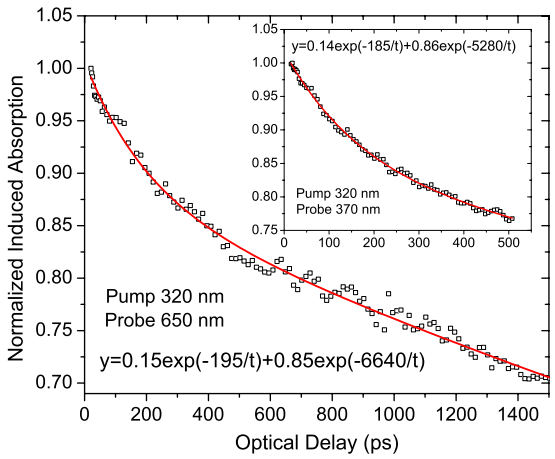

FIG. 6. (Color online) A fit to the normalized transient absorption data of the NWs at excitation of 3.8 eV and probing wavelength 650 nm at absorption fluence of 300 $\mu J/cm^2$. The inset shows the fit to the data when probing at 370 nm. The fitted double exponential curves are shown as red lines.

filling is the dominant contribution and precedes for tens of picoseconds.

It is also important to point out that given the fact that transient absorption, for probing photon energies smaller than the band edge, is identical for 3.8 and 3.1 eV excitation photons, one may conclude that the observed positive free carrier absorption signal comes from energy states located within the band gap. The possibility of free-carrier absorption signal coming from the bottom of the conduction band is excluded given that under such conditions state filling will be expected to be the dominant effect with all the photogenerated carriers accumulating at the bottom of the band.

A closer look at the transient absorption data reveals that the peak of free-carrier absorption occurs at a delay of approximately 5 ps from the excitation pulse and a fast partial recovery (only 10% of the peak value) occurs at ≈12 ps from $t=0$. This behavior is independent of the incident fluence thus it is a characteristic time of the material and is attributed to free-carrier absorption that arises from photogenerated carriers as they move from the excitation region to the long lived states which are located below the band edge. The small recovery, seen very clearly at 430 nm, is due to the capture of some of these carriers by nearby surface-related states/traps thus reducing the free-carrier absorption signal.

To obtain a better understanding of the dynamics in this nanostructured material we performed intensity measurements for different probing wavelengths. Typical results are shown in Fig. 5 where the probing wavelength was set at 370 nm and the estimated absorption fluence ranged from 550 to 11 $\mu J/cm^2$. What is important to point out here is the identical behavior of the temporal response for the range of fluences used in this work. This is clearly seen in the inset where normalized transient absorption measurements are depicted with all the curves falling on top of each other. Also seen is the linear increase in the induced absorption with increasing fluence for all optical delays. Furthermore, intensity measurements with probing wavelengths below the band edge also show the same behavior where the temporal response is identical for all the fluences and the induced absorption has a linear dependence on the fluences. These measurements suggest that nonlinear effects such as Auger recombination have a negligible role in the dynamics of these NWs even for the highest fluence of 550 $\mu J/cm^2$ used in this work.

A multiexponential fit to the transient absorption data show a minimum requirement of two exponential functions for a good fit. The fast time constant has a range between 180 and 220 ps with a coefficient ~10%–15% whereas the slow time constant has a range of 5–8 ns (90%–85%). Typical fits to the normalized transient absorption data obtained at 320 nm excitation with 650 and 370 nm probing at ~300 $\mu J/cm^2$ are shown in Fig. 6. The fitted exponential equations are also displayed with the time constants in units of ps. Most likely the fast time constant is associated with carriers moving into the various surface states or traps within the band gap whereas the long decay is associated with recombination of the carriers.

IV. CONCLUSIONS

In conclusion, we have investigated the dynamic behavior of carrier relaxation in Sn_xN_y NWs using UV femtosecond pulses with above band gap excitation. From steady state transmission measurements we estimate the band gap to be ≈2.9 eV and find an absorption band below the band edge. This absorption band appears to play an important role in the relaxation of the photogenerated carriers in the Sn_xN_y NWs. Transient differential absorption measurements reveal that strong free-carrier absorption dominates state filling at ≈0.5 ps for probing photon energies larger than the band gap. This appears to be true even for degenerate measurements and is a unique and markedly different behavior compared to what we have observed in other semiconductor NWs, e.g., InN, GaN, In_2O_3, and SnO_2. We attribute this behavior to fast scattering of the photogenerated carriers out of the excitation energy region and a possible rise in the lattice temperature due to energy relaxation. Multiexponential fits to the data reveal a minimum two exponential func-

tion for a best fit, suggesting two main channels of relaxation for the photogenerated carriers. The first channel is a relatively small component, corresponding to ≈10% of the carriers, with a time constant of approximately ~200 ps and is associated with the relaxation of the photogenerated carriers to the various surfaces/traps states. The second channel is the main component, i.e., ≈90% of the carriers, with a time constant ranging between 5 and 8 ns which is more likely associated with recombination of the recombination of electrons with holes. Intensity measurements suggest that Auger recombination has a negligible contribution to the carrier dynamics even for the highest fluence used in this work i.e., ≈550 $\mu J/cm^2$.

ACKNOWLEDGMENTS

The work in this article was supported by the Research Promotion Foundation of Cyprus under Grant Nos. EPYNE/0506/02, EPYAN/0506/04, and BE0308/03 for fundamental research in the area of nanotechnology and nanomaterials.

[1]S. Seo, G. Y. Zhao, and D. Pavlidis, Electron. Lett. **44**, 244 (2008).
[2]Y. Taniyasu, M. Kasu, and T. Makimoto, Nature (London) **441**, 325 (2006).
[3]S. Nakamura, T. Mukai, and M. Sengh, Appl. Phys. Lett. **64**, 1687 (1994).
[4]J. Wu, W. Walukiewicz, K. M. Yu, J. W. Ager, E. E. Haller, H. Lu, W. J. Schaff, Y. Saito, and Y. Nanishi, Appl. Phys. Lett. **80**, 3967 (2002).
[5]J. Li, K. B. Nam, M. L. Nakarmi, J. Y. Lin, H. X. Jiang, P. Carrier, and S.-H. Wei, Appl. Phys. Lett. **83**, 5163 (2003).
[6]M. Yang, S. J. Wang, Y. P. Feng, G. W. Peng, and Y. Y. Sun, J. Appl. Phys. **102**, 013507 (2007).
[7]F.Fischer and G. Iliovichi, Ber. Dtsch. Chem. Ges. B **41**, 3802 (1908); **42**, 527 (1909).
[8]T. Lindgren, M. Larsson, and S.-E. Lindquist, Proceedings of the 14th International Workshop on Quantum Solar Energy Conversion, 2002 (unpublished).
[9]R. G. Gordon, D. M. Hoffman, and U. Riaz, Chem. Mater. **4**, 68 (1992).
[10]N. Takahashi, K. Terada, and T. Nakamura, J. Mater. Sci. Lett. **20**, 227 (2001).
[11]D. M. Hoffman, S. P. Rangarajan, S. D. Athavale, D. J. Economou, J.-R. Liu, Z. Zheng, and W.-K. Chu, J. Vac. Sci. Technol. A **13**, 820 (1995).
[12]Y. Inoue, M. Nomiya, and O. Takai, Vacuum **51**, 673 (1998).
[13]R. Kamei, T. Migita, T. Tanaka, and K. Kawabata, Vacuum **59**, 764 (2000).
[14]L. Maya, J. Vac. Sci. Technol. A **11**, 604 (1993).
[15]R. S. Lima, P. H. Dionisio, and W. H. Schreiner, Solid State Commun. **79**, 395 (1991).
[16]B. Wang and M. J. Callahan, Cryst. Growth Des. **6**, 1227 (2006).
[17]L. Maya, Inorg. Chem. **31**, 1958 (1992).
[18]N. Takahashi, M. Takekawa, T. Takahashi, T. Nakamura, M. Yoshioka, W. Inami, and Y. Kawata, Solid State Sci. **5**, 587 (2003).
[19]T. Maruyama and T. Morishita, Appl. Phys. Lett. **69**, 890 (1996).
[20]S. V. Nand, K. Ankur, K. Brijesh, and M. B. Raj, Solid State Sci. **10**, 569 (2008).
[21]M. Zervos and A. Othonos, Nanoscale Res. Lett. **4**, 1103 (2009).
[22]A. Othonos, M. Zervos, and M. Pervolaraki, Nanoscale Res. Lett. **4**, 122 (2009).
[23]A. Othonos, M. Zervos, and D. Tsokkou, Nanoscale Res. Lett. **4**, 828 (2009).
[24]D. Tsokkou, A. Othonos, and M. Zervos, J. Appl. Phys. **106**, 084307 (2009).
[25]A. Othonos, J. Appl. Phys. **83**, 1789 (1998).